Experimental and theoretical aspects of electric-field-assisted positron kinetics in metal-oxide-silicon systems

Mihail P. Petkov *

Jet Propulsion Laboratory, California Institute of Technology, 4800 Oak Grove Drive, Pasadena, CA 91109

Kelvin G. Lynn

Department of Physics, Washington State University, Pullman, WA 99164

A. van Veen

IRI, Delft University of Technology, P.O. Box 5042, 2600AG Delft, The Netherlands

PACS: 78.70.Bj 71.60.+z 72.90.+y 68.35.-p

* Electronic mail: Mihail.P.Petkov@jpl.nasa.gov

ABSTRACT

We use positron annihilation spectroscopy to study positron kinetics in electrically-biased metal-oxide-silicon (MOS) system and trapping at the SiO_2/Si interface. Experiments carried out on samples with an extra-thick (1 μm) oxide layer reveal the electric-field-assisted positron transport in the oxide, and bring supportive evidence for the two-defect-state trapping model of the SiO_2/Si interface. The time-dependent drift-diffusion equation was solved for oxide-implanted positrons in order to obtain the fractions of positrons annihilating in the oxide and its interfaces. By fitting these results to the experimental data, the positron mobility was calculated to be $\mu_+ = 1.20 \pm 0.09$ cm^2/(V×s). This value is two orders of magnitude larger than that previously reported by Y. Kong *et al.* [*J. Appl. Phys.* **70**, 2874 (1991)], indicating distinct oxide properties. We address the mutually contradictive existing theoretical models, revise the present understanding of the positron behavior in MOS systems, and propose a general interpretation of all available results from the literature.

I. INTRODUCTION

Historically, the development of faster and smaller microelectronic products involves shrinking of the feature size (an individual transistor) thus decreasing the transistor gate delay. In the present state-of-the-art devices, the insulating layers of metal-oxide-silicon (MOS) devices are 2-3 nm thick. Serious reliability-related problems emerge for thinner oxide layers. Inevitably, the knowledge of the properties of all individual components of a MOS system becomes vital for further progress. For many decades, strong attention is devoted to the SiO_2/Si interface [1-3], whose structure is still being disputed [4,5].

Positron annihilation spectroscopy (PAS) is an established defect characterization method [6,7]. PAS has enormous defect sensitivity, originating from the ability of a positron to 'seek' open-volume defects during its random walk in the material, and become localized in them. The detected radiation emitted upon annihilation with an electron carries information about the electronic environment. In addition, low-energy positron beams enabling control over the probed depth, make PAS perfectly suited for studying thin films, multi-layered structures, and buried interfaces.

After PAS was first applied to study MOS devices [8], a wealth of information about the SiO_2 and SiO_2/Si structure and properties was obtained by two groups: at Brookhaven National Laboratory [9,10] and the Delft University of Technology [11]. Although their efforts led to a general understanding of the positron behavior in MOS, differences in the experimental results led to discrepancies in the interpretation of some key characteristics of the SiO_2 and SiO_2/Si.

The Brookhaven research identified the SiO_2/Si interface as a perfect absorber for positrons. Strong evidence was provided by (1) correlation between the evolutions of interface signal and MOS capacitance with time [9], (2) correlation with the forming gas (FG) anneal effect [12] on the interface signal [9], and (3) the measured small positron mobility in SiO_2 [13]. Based on these findings, a two-defect-state trapping model was postulated for the SiO_2/Si interface [9], considering a competition between Si dangling bonds (D) and voids. The negatively charged D^- dominate the positron trapping rate, unless passivated by FG or holes, in which case positrons probe the open volume at the interface. Additional support was obtained from the frequency dependence of the annihilation signal, related to the trapping of holes at the interface [14].

On the other hand, the Delft group demonstrated electric-field-assisted positron transport in the SiO_2 layer of a MOS device [11,15,16]. The most overwhelming evidence comes from substrate positron implantation at reverse bias, for which the annihilation signal depends on the gate metal (Al, Au, or W). This clearly shows that after overcoming the SiO_2/Si traps, positrons are transported back to the gate throughout the whole SiO_2 layer.

The theoretical models of the two groups are mutually exclusive. The major discrepancy is directly related to the positron mobility in the SiO_2. If positrons were capable of drifting in the SiO_2 of the MOS devices, studied by the Brookhaven group, all of the characteristics derived for reverse bias have to be attributed to the Al/SiO_2 interface, rather than SiO_2/Si. Then the established correlation with numerous other techniques must be ruled purely coincidental. In the opposite case, assuming that positrons do not drift in the oxide comes short of explaining the gate metal dependence,

shown in the Delft experiments. Although both theories are consistent within all of the results of the respective group, the attempts of explaining the apparent contradictory failed to achieve satisfaction.

In the present work we resolve these contradictions. Studies of "extra-thick" 1-μm-thick MOS devices, prepared at the Delft University of Technology, was carried out at Brookhaven National Laboratory. New analytical approaches are utilized to bring a direct evidence of electric-field-assisted positron kinetics, as well as a proof of the two-defect-state model. Our unified model of the MOS system, consistent with *all* existing results from the literature, reconfirms the conclusions of both, the Brookhaven and the Delft groups.

II. EXPERIMENT

Doppler broadening experiments were performed with the variable energy positron beam at Brookhaven National Laboratory [17], providing monoenergetic positrons with rate $\sim 2\times10^4$ s^{-1} (5 mm diameter) within the range from 0 to 70 keV. Shape- (*S*) and wing- (*W*) parameters are utilized in the analysis [6]. They were normalized to the averaged bulk Si values from the *n*-MOS scans for energies greater than 50 keV. All measurements are performed at room temperature in dark environment.

The samples were produced at the Delft Institute of Microelectronics and Submicron Technology (DIMES) in collaboration with the Interfaculty Reactor Institute (IRI), Delft University of Technology, the Netherlands. The *n*-MOS structure was built on *n*-type (phosphorus doped, 85 Ω×cm) Si(100) substrate (100-mm wafers #4-2 and #4-4). Extra-thick insulating SiO_2 layer was grown in water ambient at 1050 °C to a

thickness of 1 μm. MOS devices with large Al gates (12.5 mm in diameter, approximately 20-nm-thick) were built onto the SiO_2 film, and a blanket Al layer was deposited onto the back side of the wafers. The contacts were made through a mask by physical vapor deposition of Al, heated in a resistive tungsten crucible. The wafers were not subjected to forming gas anneal.

To ensure the integrity of the *n*-MOS structure, the current through the capacitors was constantly monitored not to exceed a few nano-Amperes. A pre-breakdown stage was encountered around 300 V bias (electric field of ~3 MV/cm). Although the current was in the 3-4 nA range, strong residual electric field across the oxide was present for about two hours after the bias was eliminated. Hereafter, the experimental results taken during that stage are not reported.

III. RESULTS

1. Fixed gate bias: S versus beam energy

The results from the Doppler broadening depth-profiling of the 1 μm *n*-MOS devices for bias (potential is applied to the front gate, the back side is grounded) ranging between –250 V and +250 V are shown in Figure 1. The *S*-parameter is plotted versus the mean implantation depth, *z*, determined by the empirical formula [6]: $z[\mathrm{nm}] = (40/\rho) \times E^{1.6}[\mathrm{keV}]$, where the value for the material density, ρ, was taken to be equal to that of Si (2.33 g/cm^3). Usually, the SiO_2 density in MOS structures ranges between 2.1 g/cm^3 and 2.3 g/cm^3, depending on the deposition conditions. The maximum positive bias translates into an intrinsic electric field, *E*, with a magnitude of 2.5 MV/cm, localized in the insulating oxide.

S-profiles are often used to demonstrate that positron kinetics are influenced by the presence of electric field. Extensive studies of thinner (~0.1 μm or less) MOS devices have been carried out for fields up to 3-5 MV/cm. The interpretation of these data, however, is not straightforward, and sometimes not unique. As less than 100% of the positrons are implanted in the oxide layer, the unavoidable contributions from other positron annihilation states complicate the analysis.

For our samples, at 6 keV beam energy nearly all positrons achieve thermal equilibrium in the 1 μm-thick SiO_2 layer (Figure 2). Assuming that prior to annihilation the 6-keV implanted positrons were localized in open-volume defects in the oxide network, the experimental *S*-value at that beam energy would be independent of the external bias. This contradicts the experimental observation, which is therefore a clear evidence for electric-field-assisted positron kinetics.

2. Fixed incident positron energy: S and W versus gate bias

Doppler spectra were also collected at chosen beam energies, in order to reveal the *S* and *W* dependence on the gate bias, while keeping the positron implantation conditions identical. Shown in (Figure 3) are the results for 2.5 keV (stars), 6 keV (circles), 13 keV (squares) and 20 keV (triangles). At 2.5 keV the positrons probe the area close to the Al gate ($z \approx 80$ nm). Contributions from the annihilation states at the surface and in the Al gate are seen in the spectra, and they will not be used later in the analysis. Nevertheless, these data indicate that in sufficiently strong electric field the positrons can be transported toward the substrate, across large distances (>1 μm). The jump in *S* and *W* at near zero bias will be explained later.

Figure 2 shows the calculated positron implantation profiles in a 1-μm MOS structure, for incident positron energies of 6 keV (dashed line), 13 keV (solid line), and 20 keV (dotted line). The estimated fractions of the oxide-implanted positrons, 100%, 54% and 18%, respectively, are also given. The results from the 6-keV-implantation are used to obtain the characteristics of the trapping centers in the SiO_2, as well as at the two interfaces, with the Al gate and with the Si substrate. The interface implantation (13 keV, $z \approx 1$ μm) provides the maximum sensitivity to the trapping sites at the SiO_2/Si interface, and serves the purpose to reexamine the two-state trapping model. Higher energy implantation (e.g., 20 keV) is carried out to check the consistency of the model interpretation, and also demonstrate that the positrons can be drifted back to the Al gate in strong electric fields (negative bias).

IV. ANALYSIS AND DISCUSSION

A. Oxide implantation

1. WS-analysis: potential and concerns

Simultaneous analysis of S and W recently emerged as a powerful approach for the recognition of positron annihilation states, by their S and W 'fingerprints' (for example, see Ref. [16]). If all positrons annihilate in the same state, the Doppler spectrum is independent of their spatial distribution in the sample, and thereby yields the characteristic S- and W-values for that state. Further, if a homogeneous sample contains a fixed distribution of a number of states, S and W, although containing contributions from all participating states, are again, characteristic for the probed material. In a depth-profiling of a layered structure, the experimentally observed S and W are, by definition,

linear combinations of the specific S and W of each layer (S_n and W_n in the n-th layer), weighted with the respective normalized fractions, f_n ($\sum_n f_n = 1$), of the positrons probing them:

$$S = \sum_n f_n S_n \ , \tag{1}$$

and $$W = \sum_n f_n W_n \ . \tag{2}$$

Equations (1) and (2), along with the normalization condition, limit the maximum number of layers, for which the results can be unambiguously resolved, to three. (In rare cases, the positronium parameter, R [6], can be included as an additional condition to resolve four layers.) Although partial information about available distinct states can be obtained, complications arise when the distinct areas are more than three. This is certainly the case of positron beam profiling of *thin* MOS structures. The broad positron distribution after thermalization (Figure 2) and the additional spread due to thermal diffusion cause simultaneous probing of all or several of the various regions: surface, gate, gate/SiO_2 interface, SiO_2, SiO_2/Si interface, and Si substrate. Furthermore, earlier studies [9] reported a change in the interface characteristics depending on the polarity of the bias (as compared to V_{fb}), due to change in the charge state of the traps.

Changes in the beam energy causes a redistribution of the weights for each participating state, which affects the experimentally measured annihilation parameters. This obscures the effect of the electric field on the positron kinetics, which is the main subject of study in our experiments. To avoid concerns over the interpretation of our SW-data, we favored data collection at several fixed beam energies, while varying the gate bias (Figure 3). This method has two major advantages. First, the number of probed distinct layers is greatly reduced (in most cases down to three), allowing the

unambiguous identification of their S and W 'fingerprints'. And second, the initial positron distribution in each layer is kept identical, which eliminates its unwanted influence on the experimental results.

2. Mapping positron annihilation states

The 100% oxide implantation (6 keV), combined with the positron mobility in electric field can be utilized to map the specific S and W of the Al/SiO_2 interface, the bulk SiO_2, and the SiO_2/Si interface, in addition to the known values for the substrate ($S = W = 1$). Figure 4 shows the S and W results from Figure 3 (6 keV), plotted against each other independent on the gate bias. The dashed arrows indicate the trend of the changes of the WS-pairs with the increase of the bias magnitude (positive or negative).

The oxide-implanted positrons are drifted toward the Si substrate with positive bias applied to the gate. When its magnitude exceeds 150 V, both S and W no longer change, and reveal the 'fingerprint' of the SiO_2/Si interface: $(S;W)_{\mathrm{Si-int}} = (0.927;1.645)$. Even at the largest value of the applied bias, the (S; W)-pairs do not show any tendency of shifting toward the Si point $(S;W)_{\mathrm{Si}} = (1;1)$. This proves that the positrons cannot gain sufficient energy to overcome the potential barrier in order to penetrate the Si substrate, in agreement with all previous studies of thinner MOS devices.

Vice-versa, for large negative bias ($V < -200$ V) all positrons are transported back to the Al/SiO_2 interface, and its $(S;W)_{Al-\mathrm{int}} = (1.032;1.031)$ characteristic point is obtained. We must emphasize that these experiments cannot conclusively determine whether the positrons annihilate in the Al gate or at its interface with the oxide layer. Annihilation in the gate cannot be clearly resolved because of its small thickness.

B. Theoretical model

1. Time dependent drift-diffusion equation

In the absence of electric field, the motion of thermal positrons in a solid is well described by a simple diffusion equation [6]. Introduction of electric field is achieved in the drift-diffusion approximation, by analogy with the familiar classical carrier transport models [18]. Thus, the motion of the SiO_2-implanted positrons under the influence of the electric field is described by the following drift-diffusion equation (DDE):

$$\frac{\partial n(\boldsymbol{r},t)}{\partial t} = D_+ \nabla^2 n(\boldsymbol{r},t) - \nabla \cdot [n(\boldsymbol{r},t)\boldsymbol{w}] - \lambda n(\boldsymbol{r},t) \quad , \tag{3}$$

where $n(\boldsymbol{r},t)$ is the positron density function, D_+ – the positron diffusion coefficient in SiO_2, $\boldsymbol{w}$ – their drift velocity and λ – the annihilation rate. The drift velocity, which enters in the electric-field term, can be expressed as function of the electric field $\boldsymbol{E}$:

$$\boldsymbol{w} = \mu_+ \boldsymbol{E} \quad , \tag{4}$$

where μ_+ is the positron mobility at small fields. This holds for small $|\boldsymbol{w}|$ in comparison to the thermal velocity, $v_0 = 9.5 \times 10^6$ cm/s. Eq. 3 is converted to the simple diffusion equation in the transverse to $\boldsymbol{E}$ direction, in which the effect of the electric field is negligible (e.g., positron drift experiments in Si [19] were insensitive to Doppler-shift changes in the transverse direction). This allows us to reduce the spatial variables to one, along which the field is applied.

The time-dependence in the DDE is often eliminated using the quasi-stationary approximation, which gives satisfactory results [13,20]. Here, we will work with the time-dependent DDE, and the exact space- and time-dependent solutions will be integrated in the end as needed.

We set the initial conditions by the Makhovian positron implantation profile:

$$n(z,0) = \frac{2z}{z_0^2} e^{-\left(\frac{z}{z_0}\right)^2} \quad , \tag{5}$$

where z_0 = 330 nm is the mean implantation depth at 6 keV. Further, both interfaces (Al/SiO_2 and SiO_2/Si) enclosing the oxide layer were assumed abrupt and were modeled

$$\begin{aligned} J_{Al/SiO_2}(t) &= D_+ \frac{\partial n(z,t)}{\partial z}\Big|_{z=0} + wn(0,t) = \eta n(0,t) \\ J_{SiO_2/Si}(t) &= D_+ \frac{\partial n(z,t)}{\partial z}\Big|_{z=d} - wn(d,t) = \eta n(d,t) \end{aligned} \tag{6}$$

by perfect positron absorbers (both having positron trapping rate $\eta = \infty$):

A rough estimate of the validity of this approximation can be made by taking the lower bounds of the interface trapping rate (10^{15} s^{-1}) and interface thickness (the length of Si-O bond at SiO_2/Si interface, 0.166 nm [21]). This sets an upper limit on the positron energies to $\sim 10k_BT$. As we will demonstrate, in our experiments the positrons gain little energy even at the maximum achieved field ($\Delta E \ll k_BT$), and therefore, for oxide-implantation, it is safe to consider both interfaces as perfect sinks.

Figure 5 illustrates a schematic diagram of the electric potentials in a MOS structure as experienced by positrons (left), and the evolution of the positron density function (PDF) in the oxide (right). The PDF is the solution of the time-dependent DDE for fixed μ_+ and E. Positrons are implanted at 6 keV through the Al gate, and the PDF at $t = 0$ gives the implantation profile in the 1 μm oxide; the arrow in "Al → Si" (3D-figure, right) indicates increasing depth. The PDF time evolution is followed for a period of one lifetime, τ (τ = 270 ps [22]). Part (a) shows the flat-band conditions, at which DDE is

converted to a simple diffusion equation (E = 0). Parts (b) and (c) demonstrate the positron drift in the oxide, which occurs when an electric field is applied.

2. Fitting parameters and procedures

Electric-field-assisted drift in the oxide was observed at very weak fields, which implies that the positrons are not localized. It can be then assumed that the positron annihilation rate in the oxide is similar to that of free positrons in a quartz crystal ($\lambda = 1/\tau_b$, $\tau_b = 270$ ps [22]).

The DDE can be solved for any set of D_+ and μ_+ values. A close inspection, however, shows that large variations of D_+ cause little change in the quality of the final fits, thus indicating large uncertainties of the D_+ determination. Measurements of positron diffusion length bring no additional help, as neither the defect density, nor their specific trapping rate is known. We can than relate D_+ and μ_+ by the Nernst-Einstein relation (e is the unit charge):

$$D_+ = \frac{k_B T}{e} \mu_+ \quad , \tag{7}$$

in which way only one free parameter remains in the DDE. It is worth mentioning that the calculated values of D_+ through μ_+ are well within the range obtained by fitting as an independent parameter.

Special care has to be taken to evaluate properly the magnitude of the electric field. First, MOS devices have built-in electric potential, caused by the mismatch of the Al and Si work functions, which can be compensated by applying a potential V_{fb} (flat-band voltage) to the gate. In our devices $V_{fb} \approx$ -9 V, as measured by capacitance-voltage (CV) technique. This value also accounts for the eventual presence of uniformly distributed fixed charges in the SiO_2, caused by impurities. And second, the magnitude of the electric field in the oxide is affected by the regime in which the MOS operates,

which in turn depends on the substrate type and the polarity of the applied bias with respect to V_{fb}.

2.1. Accumulation ($V > V_{fb}$)

A simple evaluation of the electric field in *n*-type MOS can be done for positive bias (more precisely, $V > V_{fb}$), a regime known as *accumulation*. The majority carriers in *n*-type Si (electrons) are driven from within the substrate back to the SiO_2/Si interface, where they accumulate. The high density of negative charges results in screening of the electric field from the substrate. The potential across the oxide changes linearly (Figure 6, accumulation) and the electric field, given by $E = (V - V_{fb})/d$ (d is the oxide thickness), is constant with depth.

The fitting procedure enables the reconstruction of the experimentally observed W-parameter as a function of the electric field by solving the DDE for the proper mobility. W was preferred because the ratio of the statistical error and the difference between the respective oxide and interface values was significantly smaller than that obtained from the S-parameter (Figure 3).

Active fitting of our model to the experimental data is principally possible, but requires a large amount of computer time. Instead, we created a family of curves, solutions of the time-dependent DDE for a fixed μ_+ for a range of E values (0-2.5 MV/cm). Integration over time and depth yielded the fractions of the positrons, annihilating in the oxide and at the SiO_2/Si interface, f_{ox} and f_{int}, respectively, which were used to model W. The characteristic oxide value of W was determined experimentally at 6 keV beam energy on bare oxide samples from the same wafer. As the experiments

alone cannot confirm that *all* positrons annihilate at the SiO_2/Si interface at the largest achieved bias, that W-signature was left as a free parameter.

Figure 7(a) shows the calculated W for some values of μ_+, optimized by means of least square fit to the data. Clearly, the time-dependent DDE model of the electric-field-assisted positron transport is capable of reconstructing the experimentally observed features. In the studied range of μ_+, the goodness of the fit, χ^2, takes the values of 10.2 for $\mu_+ = 0.6$ cm^2/(V×s) and 5.3 for $\mu_+ = 2.0$ cm^2/(V×s). Best fit ($\chi^2 = 2.2$) is obtained for $\mu_+ = 1.20 \pm 0.09$ cm^2/(V×s), for which the error is estimated from the uncertainties in the fitted parameters. Although χ^2 is strongly affected by the small difference in the characteristic W-parameters of the oxide and the SiO_2/Si interface, the deviations from the $\mu_+ = 1.2$ cm^2/(V×s) curve appear to be random, rather than systematic (Figure 7(a), solid line).

For the purpose of this work, the precision in the mobility is sufficient to carry out a comparison with previously reported values. Moreover, as we will demonstrate in the course of discussion, this μ_+ is not as characteristic for SiO_2 as mobility values measured in crystals, the reasons for which can be traced back to preparation conditions. If needed, the precision can be improved by decoupling D_+ and μ_+, and acquiring more data at small E values, where D_+ is important.

2.2. Depletion ($V < V_{fb}$)

More complicated is the regime of *depletion*, $V < V_{fb}$. The majority carriers are repelled deeper into the substrate forming a depleted region near the SiO_2/Si interface, in which the electric field penetrates. The most commonly used approximation of the

electric field in the depletion layer is linear attenuation from a maximum value at the interface to zero at the end of the depletion layer. This creates a change of the potential across the device as shown in Figure 6 (depletion). The main potential drop in this case is contained within the depletion layer. In our experiments, however, positrons are injected only into the oxide layer and are not affected by electric fields in the substrate. They experience electric field constant in depth as in the regime of accumulation, but with significantly smaller magnitude.

We designate ξ ($\xi < 1$) as the scaling factor of the magnitudes of the electric fields at reverse bias ($-|V - V_{fb}|$) and forward bias ($|V - V_{fb}|$), e.g. $E^- = \xi E^+$ (the superscripts denote the direction of the field). Keeping the mobility fixed to the obtained for the forward bias value, the drift velocity can be expressed as $w^- = \xi w^+$. Thus, after fixing $\mu_+ = 1.2$ cm^2/(V×s), ξ becomes the only fitting parameter for the depletion regime in a procedure identical to that of the determination of μ_+ in accumulation. $\xi = 0.147 \pm 0.007$ was obtained from a fit with $\chi^2 = 1.2$. Both, the model and the experimental results were plotted as a function of the electric field in Figure 7(b).

The significance of this fitting routine is that PAS can be used as an alternative to obtain device properties, which can be compared to those, derived by a CV technique.

C. Kinetics of the oxide-implanted positrons in electric field

Knowing the value of the positron mobility in the SiO_2, the electric-field-assisted positron kinetics can easily be understood. An energetic analysis can be carried out for positrons in a quasi-equilibrium state (average energy gain equals average energy loss) in analogy with the common methods for treating carrier properties in semiconductor

devices. Such discussion will shed light on the possibility for having ballistic positrons, which depends on the balance between the energy gains and losses while traveling through the oxide. The average energy gained from the acceleration in electric field between collisions occurs with a rate of $e^2E^2\langle t\rangle/m$, where $1/\langle t\rangle = v/l$ is the average collision rate, expressed in terms of the scattering length l, and the positron velocity, v. On the other hand, the energy loss rate is $\delta\varepsilon/\langle t\rangle$, with $\delta\varepsilon$ being the average energy loss per collision. For positrons in quasi-equilibrium we have:

$$\frac{d\varepsilon}{dt} = \frac{e^2E^2\langle t\rangle}{m} - \frac{\delta\varepsilon}{\langle t\rangle} = 0 \quad . \tag{8}$$

Remembering that the positron mobility is

$$\mu_+ = \frac{el}{mv} = \frac{e}{m}\langle t\rangle \quad , \tag{9}$$

$\delta\varepsilon$ can be expressed as

$$\delta\varepsilon = m\mu_+^2E^2 \quad . \tag{10}$$

The maximum energy loss per collision at E = 2.5 MV/cm field is $\delta\varepsilon$ = 5.1 meV. This value is within the energy range of the available acoustic phonons and significantly less than the energy of the transverse optical (TO) phonons in quartz (20-23 meV) [23], which dominate the energy loss spectrum. Therefore, the limit at which $w = \mu_+E$ no longer holds occurs at several times larger fields than the maximum achieved in our experiments.

At E = 2.5 MV/cm the drift velocity is $w = 3\times10^6$ cm/s, significantly smaller than the thermal velocity, $v = 9.5\times10^6$ cm/s. This translates into a 10% energy gain (2.6 meV,

or $0.1k_BT$) as compared to the thermal energy. Using Eqs. 9 and 10 to eliminate $\langle t \rangle$ and μ_+ in Eq. 8, the average positron kinetic energy, T, can be written as

$$T = \frac{1}{2}\frac{e^2E^2l^2}{\delta\varepsilon} \quad , \tag{11}$$

from where an average scattering length of $l = 0.07$ nm is calculated. Being smaller than the Si-O bond length in SiO_2 (0.158 nm [21]), this value indicates that positrons also undergo elastic collisions. Therefore, the average loss per collision is significantly smaller than the energy transferred in inelastic processes, which identifies the TO phonon excitation as the positron quenching mechanism in SiO_2. The calculated energy loss rate is $\delta\varepsilon / \langle t \rangle = 7\times10^{12}$ eV/s. The existence of ballistic positrons in the 1 μm-thick oxide is difficult to reconcile at this high energy-loss rate; however, significantly thinner oxides may indeed facilitate the transport of energetic positrons from the substrate into the metal gate, prior to loosing their initial energy (~1 eV).

Assuming high defect density in the SiO_2, the positron transport at relatively weak electric fields cannot be explained by any conventional means. Resonance effects are not considered, as the de Broglie wavelength of positrons with energy of $1.1k_BT$ is ~6.0 nm, almost identical to that of thermal positrons and much larger than the trap dimensions. Yet, the 10% energy gain is sufficient to impede the trapping rate for epithermal positrons, which is indicative of small defect density or shallow traps.

D. Experimental evidence for two-defect-state SiO_2/Si trapping model

1. SiO_2/Si implantation in accumulation ($V > V_{fb}$)

Having found the characteristics of the various layers from the oxide implantation experiments, we can proceed further with analysis of the defects at the SiO_2/Si interface.

Figure 8 (squares) shows W versus S at 13 keV incident beam energy, with dashed arrows indicating the trend of change of the bias. The signatures of the oxide, and the two interfaces (Al/SiO_2 and SiO_2/Si), obtained from our previous analysis are also given by large solid circles. At this energy, 53% of the positrons are implanted in the oxide and the remaining 47% are thermalized in the substrate (Figure 2). The interface thickness is ignored in these calculations. In reality, however, in the absence of intrinsic electric field ($V = V_{fb}$), annihilation at the interface is significant due to thermal diffusion of positrons from the oxide and mostly from the substrate.

In the regime of accumulation ($V > V_{fb}$), Si-implanted positrons remain unaffected by the electric field except at the SiO_2/Si, where the bending of the electric potentials prevent them from reaching the interface. Their annihilation carries the characteristic signature of bulk Si ($S = W = 1$). The remaining oxide-implanted fraction of positrons, on the other hand, is driven by the electric field toward SiO_2/Si interface in the manner discussed in the previous section, without being capable of overcoming the potential barrier to penetrate the substrate. In general, annihilation in both, SiO_2 and SiO_2/Si will contribute to the experimental spectra. In the extreme case, when at sufficiently large fields all SiO_2-implanted positrons reach the interface, the resulting spectrum is a weighted-average of the SiO_2/Si and Si signatures.

Experimental evidence of this simple linear combination of the two states is clearly seen in the WS-points at large bias ($V > 200$ V), which lie on the SiO_2/Si–Si line. This allows for a graphical determination of the SiO_2 and Si implanted fractions using either S or W. For the 13 keV-implantation, we obtain 54±1% and 46±1%, respectively, in an excellent agreement with the calculated values of 53% and 47% (Figure 2).

Similarly, the estimated from the 20 keV-data (Figure 8, triangles) 18±2% oxide-implanted positron fraction agrees well with the calculated value of 18% (Figure 2).

The benefits of using constant incident energy as opposed to fixed bias become evident in the emerging simple picture of the positron behavior in *n*-MOS, in the regime of accumulation. Only three annihilation states, SiO_2, SiO_2/Si and Si, whose S and W signatures were independently determined, are important for the reconstruction of the experimental data. Eqs. 1 and 2, along with the normalization of the weights, allow for the unambiguous determination of the contribution of each state.

The results from these calculations for 13 keV are shown in Figure 9 as a function of the gate bias (the lines are guides to the eye). Small forward bias ($V > V_{fb}$) impedes the positron diffusion from the substrate back to the interface. Annihilation in the bulk Si (solid circles) appears unaffected by the bias and remains constant at 46%, as shown for $V > 0$ V. The complementary behavior of the SiO_2 (open triangles) and SiO_2/Si fractions (open squares) is consistent with the electric-field-assisted positron transport, taking place in the oxide. The interface signal increases on the expense of the oxide annihilation.

2. SiO_2/Si implantation in depletion ($V < V_{fb}$)

So far, we have discussed only the SiO_2/Si interface signature (denoted as "SiO_2/Si +", Figure 8) at positive bias. Our simple SiO_2–SiO_2/Si–Si model can be extended to calculate the contributions from these three states at negative bias. For this, we shall assume that the characteristic SiO_2/Si signal remains unchanged by the bias (in

contrast to the findings of Ref. [9]), and redistribution of the positron fractions is solely responsible for the changes in the measured S and W.

We must emphasize that strong electric fields can lead to positron transport back to the Al/SiO_2 interface because of the large positron mobility. Such unwanted influence can be avoided if only the results for weak electric fields are considered ($E \approx 0.06$ MV/cm at V = -50 V). Judging by the 6 keV-results and the difference in the implantation profiles at 6 keV and 13 keV, the probability of drifting oxide-implanted positrons back to the gate can be ignored. For substrate-implanted positrons, on the other hand, the potential difference in the workfunctions of SiO_2 and Si (of the order of 1 eV) is transformed into kinetic energy upon entering the oxide. The calculated large energy loss rate, however, indicates that the energy of these positrons will reach equilibrium with the field after a distance of several nanometers, negligible in comparison with the oxide thickness.

The results from the calculations at negative bias and 13 keV beam energy are shown in Figure 9. Near the flat-band condition (V = -9 V) the results imply an increase of the annihilation at the SiO_2/Si interface on the expense of bulk annihilation due to back-diffusion from the Si substrate. At larger bias (V < -30 V), however, the calculated fractions are clearly erroneous: there is no logical explanation within the frames of the assumed model of the increase of the bulk signal (solid circles). As the system is well defined (three equations for three unknowns) and a contribution of a fourth state is eliminated, we must conclude that our initial assumption is incorrect, and the characteristics of the considered states have changed. Ruling out the Si and SiO_2 is trivial, and therefore the cause can be traced to the signature of the SiO_2/Si interface.

We can take this a step further and make a rough estimate of the (*S*; *W*) interface 'fingerprint' at negative bias. For that, we assume that for small bias (-20 V, -30 V), the fraction of positrons, driven in the direction of the interface by the electric field in the depletion layer, is small in comparison with the fraction of positrons, reaching the interface in the diffusion process. Equivalently, the respective weights of the participating layers are assumed to be similar to those at flat-band condition. The obtained signature is shown in Figure 8 (denoted as "SiO_2/Si –"). We must stress that the present data cannot conclusively identify the "SiO_2/Si –"-fingerprint.

V. REVISION OF THE ISSUES OF DEBATE

A positron mobility in a biased SiO_2 was found to be ~1.2 $cm^2/(V\times s)$, two orders of magnitude larger than the ~0.013 $cm^2/(V\times s)$ value, reported by Kong et al. [13]. This clearly established differences in the properties of the studied oxides reflect in the positron kinetics and, naturally, result in incompatible experimental results.

Although this conclusion explains the experimental and theoretical differences between the two groups, mobility in the SiO_2 is not often reported. A more general criterion, which can give a broader basis for comparison of the results from the literature, is needed. Doppler parameters (*S* and/or *W*) acquired as functions of the gate bias for interface implantation (constant beam energy) is an excellent reference. The results for positive bias are comprised from SiO_2, SiO_2/Si and Si contributions, with the latter one remaining constant. As the SiO_2 and SiO_2/Si signatures are drastically different [9-11, 15,16,24], any change of the experimentally measured parameters is directly related to a

positron drift from the oxide into the SiO_2/Si interface. Fortunately, numerous publications contain such data.

The present paper shows a change in both, *S* and *W* with positive bias in the 13 keV-data (interface implantation; Figure 3, squares) and the drift is evident. Refs. [9,10] contain several identical plots, presenting various aspects of the research of *n*- and *p*-type MOS (correlation with forming gas anneal, room temperature and 35 K results, light/dark experiments, etc.). None of these figures exhibits a change in the Doppler parameters with positive bias, which is consistent with the low positron mobility in the oxide measured on similar material. Drift in the oxide can be concluded from another Brookhaven work [14], studying the frequency dependence of the annihilation signal from the interface.

Depth profiling of the Doppler parameters in reverse biased MOS can be used as an alternative, though less convincing approach in assessing the electric-field-assisted positron transport in the oxide. As an example, Figure 48 in Ref. [10] shows two distinct peaks in the *S*-parameter, associated with the Al/SiO_2 and the SiO_2/Si interfaces. In case of enhanced positron mobility in the oxide, these two peaks cannot be clearly separated (Figure 1) despite the thick oxide layers of our samples.

All issues debated in the literature are easily resolved if the positron mobility in the oxide layer end the energy aspects of the positron kinetics are considered carefully.

- *Electric-field-assisted transport*

Obviously, the positron mobility is directly related to the properties of the specific oxide layer, which can most likely be traced back to preparation conditions. In the absence of strong and efficient traps, the positron drift in electric field is enhanced, as

first demonstrated by the Delft group. The examples given in this paper characterize the extremes from immobile to nearly free positrons, indicating that oxide with any desired property can be engineered.

- *SiO_2/Si approximation with a perfect positron absorber*

In general, the SiO_2/Si interface cannot be considered as a perfect sink for positrons. This is evident from the experiments carried at Delft, as well as in the present work. As we demonstrated, backward-driven from the Si to the SiO_2 positrons lose their initial energy after crossing a distance of several nanometers, after passing over the interface with a kinetic energy of the order of 1 eV. Thus, the trapping rate at the SiO_2/Si is strongly suppressed. Resonance trapping at these energies is not likely to play a significant role, as the de Broglie wavelength of 1 eV positrons is ~1.0 nm, larger than the size of the divacancies decorating the interface [24].

The Brookhaven experiments, on the other hand, do not support positron transport in the SiO_2 layer due to a significantly larger energy loss rate. Having in mind that the positron mobility is proportional to the average time between collisions (Eq. 9), the energy loss rate goes as $\delta\varepsilon/\mu_+$. In a similar to the discussed above analysis, we take the reported values in Ref. [13] for the maximum field (3.3 MV/cm) and calculate $\delta\varepsilon \approx 10.5$ meV, a factor of 2 larger than that in our samples, but still below the TO phonon limit (20-23 meV, [23]). Thus, in conjunction with the 100 times smaller mobility, we find that their energy loss rate is some 200 times larger than the estimated from our experiments. Therefore, all positrons approaching the interface from the substrate remain trapped in the defects at the SiO_2/Si, and thereby it is safe to consider that in that system the interface is a perfect sink for positrons.

- *Two distinct defect signatures at the SiO_2/Si interface*

In our experiments, the interface signature at negative bias is weak, obscured by the finite trapping rate at the SiO_2/Si, and the consequences of the positron transport in the oxide. Nevertheless, the analysis confirms the bias-dependent two-defect-state model of the SiO_2/Si interface, proposed by the Brookhaven group. The lack of positron mobility in their samples enabled the investigation of a broad spectrum of SiO_2/Si properties without such complications. The dominant role in the positron trapping at the SiO_2/Si in a forward biased MOS was attributed to the negatively charged Si dangling bonds. A somewhat less specific description was given of the neutral defects, responsible for the interface annihilation signal at reverse biased MOS. A recent work by Kauppinen *et al.* [24] gives more insight by identifying divacancies at the SiO_2/Si interface.

VI. SUMMARY

In the present work, we clearly demonstrated the field-assisted positron transport generated by electric fields with a magnitude of as little as ~0.1 MV/cm. A theoretical model, based on the time-dependent drift-diffusion equation, was used to calculate a positron mobility of $\mu_+ = 1.20 \pm 0.09$ cm^2/(V×s). This value was used to perform a detailed analysis of the positron kinetics in electrically biased MOS system. Drift velocity (3×10^6 cm/s), energy gain ($0.1k_BT$), average loss per collision (5.1 meV), and energy loss rate (7×10^{12} eV/s) were estimated at the maximum achieved electric field (2.5 MV/cm) in our experiments.

Evidence of bias-dependent two-state signature of the SiO_2/Si was obtained for interface positron implantation, despite the destructive interference of the relatively small energy loss rate and enhanced positron mobility in the oxide.

We applied our energetic approach to resolve long-debated aspects of the positron kinetics in MOS systems, and provide justification of previously reported in the literature results. We conclude that the contradictions originated from the failure to consider properly the oxide properties, which govern the positron mobility and the energy loss rate. Estimates and comparison of these quantities with our values is performed.

Our findings can be utilized for further progress in characterizing the defect states at the SiO_2/Si interface by means of two-dimensional angular correlation technique (2D-ACAR), imaging the electron momentum space. MOS devices with high and low positron mobility in the SiO_2 can be engineered. The former can provide the signature of the Si dangling bonds (thick oxide, SiO_2 implantation, forward bias), whereas the latter can be used to obtain the divacancy 'fingerprint' (thin oxide, substrate implantation in high-resistivity Si, reverse bias).

In conclusion, we resolved prior debates on the interpretation of the experimental results from positron studies of MOS systems. This paves the way for further progress in the understanding of the SiO_2/Si structure and properties, important for the future progress in fabricating state-of-the-art thin-gate transistors.

ACKNOWLEDGEMENTS

We are indebted to P. Asoka-Kumar, B. Nielsen, J.M.M. de Nijs, M. Clement and H. Schut for their valuable discussions and comments. We also thank B. Nielsen for making the positron facility at Brookhaven National Laboratory available for these studies. The research was supported by the Division of Materials Science, U.S. DOE – Basic Energy Science, and DIMES-STW, Delft, the Netherlands. Publication support was provided by the Jet Propulsion Laboratory, California Institute of Technology, under a contract with National Aeronautics and Space Administration.

REFERENCES

1 *SiO_2 and Its Interfaces*, edited by S. T. Pantelides and G. Lucovsky, *MRS Symposia Proceedings No. 105* (Materials Research Society, Pittsburgh, 1988).

2 *The Physics and Chemistry of SiO_2 and Si-SiO_2 interface*, edited by R.C. Helms and B.E. Deal (Plenum, New York, 1988); *The Physics and Chemistry of SiO_2 and Si-SiO_2 interface 2*, edited by R.C. Helms and B.E. Deal (Plenum, New York, 1993).

3 A. Pasquarello, M.S. Hybertsen, and R. Car, *Nature* **396**, 58 (1998).

4 M.M. Banaszak Holl and F.R. McFeely, *Phys. Rev. Lett.* **71**, 2441 (1993).

5 M.M. Banaszak Holl, S. Lee, and F.R. McFeely, *Appl. Phys. Lett.* **65**, 1097 (1994).

6 P. Schultz and K.G. Lynn, *Rev. Mod. Phys.* **60**, 701 (1988).

7 M.J. Puska and R.M. Niemenen, *Rev. Mod. Phys.* **66**, 841 (1994).

8 A. Uedono, S. Tanigawa, and Y. Ohji, *Phys. Lett. A* **133**, 82 (1988).

9 T.C. Leung, P. Asoka-Kumar, B. Nielsen, and K.G. Lynn, *J. Appl. Phys.* **73**, 168 (1993).

10 P. Asoka-Kumar, K.G. Lynn, and D.O. Welch, *J. Appl. Phys.* **76**, 4935 (1994).

11 M. Clement, J.M.M. de Nijs, P. Balk, H. Schut, and A. van Veen, *J. Appl. Phys.* **81**, 1943 (1997).

12 E.H. Nicollian and J.R. Brews, *MOS Physics and Technology* (Wiley, New York, 1982).

13 Y. Kong, T.C. Leung, P. Asoka-Kumar, B. Nielsen, and K.G. Lynn, *J. Appl. Phys.* **70**, 2874 (1991).

14 H.L. Au, P. Asoka-Kumar, C.D. Beling, S. Fung, and K.G. Lynn, *Phys. Stat. Sol. B* **178**, K11 (1993).

15 M. Clement, J.M.M. de Nijs, A. van Veen, H. Schut, and P. Balk, *IEEE Trans. Nucl. Sci.* **NS-42**, 1717 (1995).

16 Maarten Clement, *Ph.D. Dissertation*, (Delft University Press, Delft, the Netherlands, 1998), Chapter 4.

17 K.G. Lynn, B. Nielsen, and J.H. Quateman, *Appl. Phys. Lett.* **47**, 239 (1985).

18 S.M. Sze, *Physics of Semiconductor Devices*, 2nd ed. (Wiley & Sons, New York, 1981).

19 A.P. Mills, Jr. and L. Pfeiffer, *Phys. Lett.* **63A**, 118 (1977).

20 J. Mäkinen, C. Corbel, P. Hautojärvi, A. Vehanen, and D. Mathiot, *Phys. Rev. B* **42**, 1750 (1990).

21 Z.W. Yuan, S. Csillag, M.A. Tafreshi, and C. Colliex, *Ultramicroscopy* **59**, 149 (1995).

22 Y. Nagai, Y. Nagashima, and T. Hyodo, *Phys. Rev. B*, **60**, 7677 (1999).

23 A.N. Lazarev, A.P. Mirgorodsky, *Physics and Chemistry of Minerals* **18**, 231 (1991).

24 H. Kauppinen, C. Corbel, L. Liszkay, T. Laine, J. Oila, K. Saarinen, P. Hautojärvi, M.-F. Barthe, and G. Blondiaux, *J. Phys.: Condens. Matter* **9**, 10595 (1997).

FIGURE CAPTIONS

Fig. 1 *S* parameter as a function of depth at different gate bias.

Fig. 2 Positron implantation profiles at chosen beam energies: 6 keV – dashed line; 13 keV – solid line; 20 keV – dotted line. The oxide-implanted fraction of positrons is also given.

Fig. 3 *S* and *W* parameters versus gate bias at chosen energies.

Fig. 4 *WS*-plot for field-driven oxide-implanted positrons, showing distinct positron annihilation states (Al/SiO_2, SiO_2, and SiO_2/Si).

Fig. 5 Left: Electric potentials in a MOS device as experienced by positrons at (a) flat-band condition ($V = V_{fb}$), (b) forward bias ($V > V_{fb}$), and (c) reverse bias ($V < V_{fb}$). Small variations in the oxide potential represent trapping centers, whereas the interface traps are shown as deep traps. The dashed lines represent the average positron energy. Right: Evolution of the positron density function within one lifetime. The solutions of the time-dependent drift-diffusion equation are calculated at the respective conditions, given to the left.

Fig. 6 Magnitude of the electric potentials in a *n*-type MOS device as a function of depth, for the regimes of accumulation and depletion.

Fig. 7 The experimental (points) and the reconstructed W-parameters (line) as a function of the electric field, E. The expanded window (a) shows W in the accumulation regime, calculated for different values of μ_+ (dashed lines), along with the best fit obtained for $\mu_+ = 1.2\ cm^2/(V\times s)$ (solid line). Part (b) shows the best fit for $\mu_+ = 1.2\ cm^2/(V\times s)$ with the re-scaled negative electric field to account for the field in the depletion layer ($\times 0.147$).

Fig. 8 WS-plot for 13 keV (squares) and 20 keV (triangles) positron implantation energy. The coordinates of the individual states are shown. "SiO_2/Si –" designates the interface signature at negative bias, calculated from the trapped positron fractions at small negative bias.

Fig. 9 Fraction of positrons, annihilating in the SiO_2 (open triangles), SiO_2/Si (open squares) and Si substrate (solid circles), versus gate bias for 13 keV beam energy. Lines for $V > 0$ are guides to the eye.

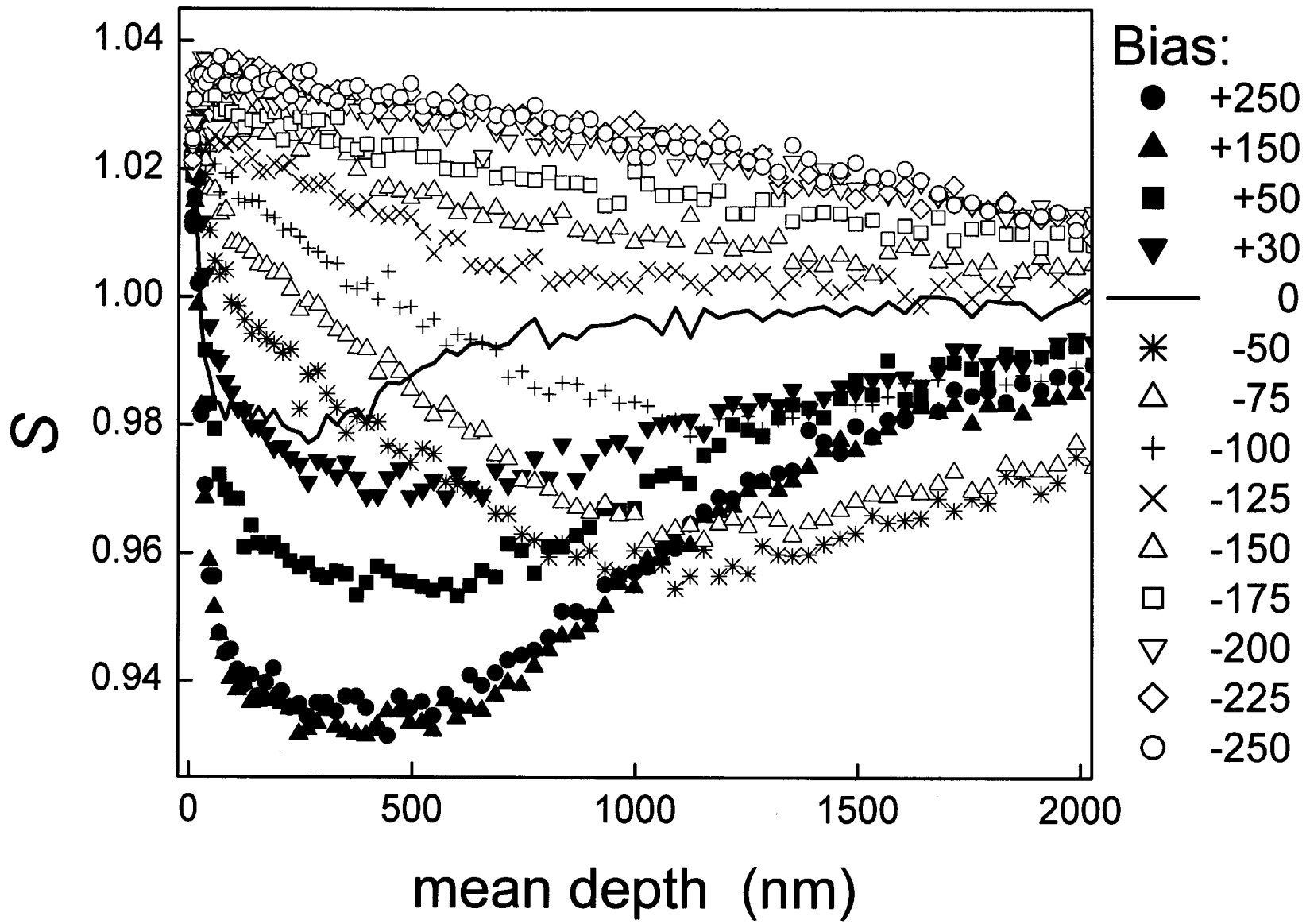

Figure 1 M.P. Petkov *et al.*, *Phys. Rev. B*

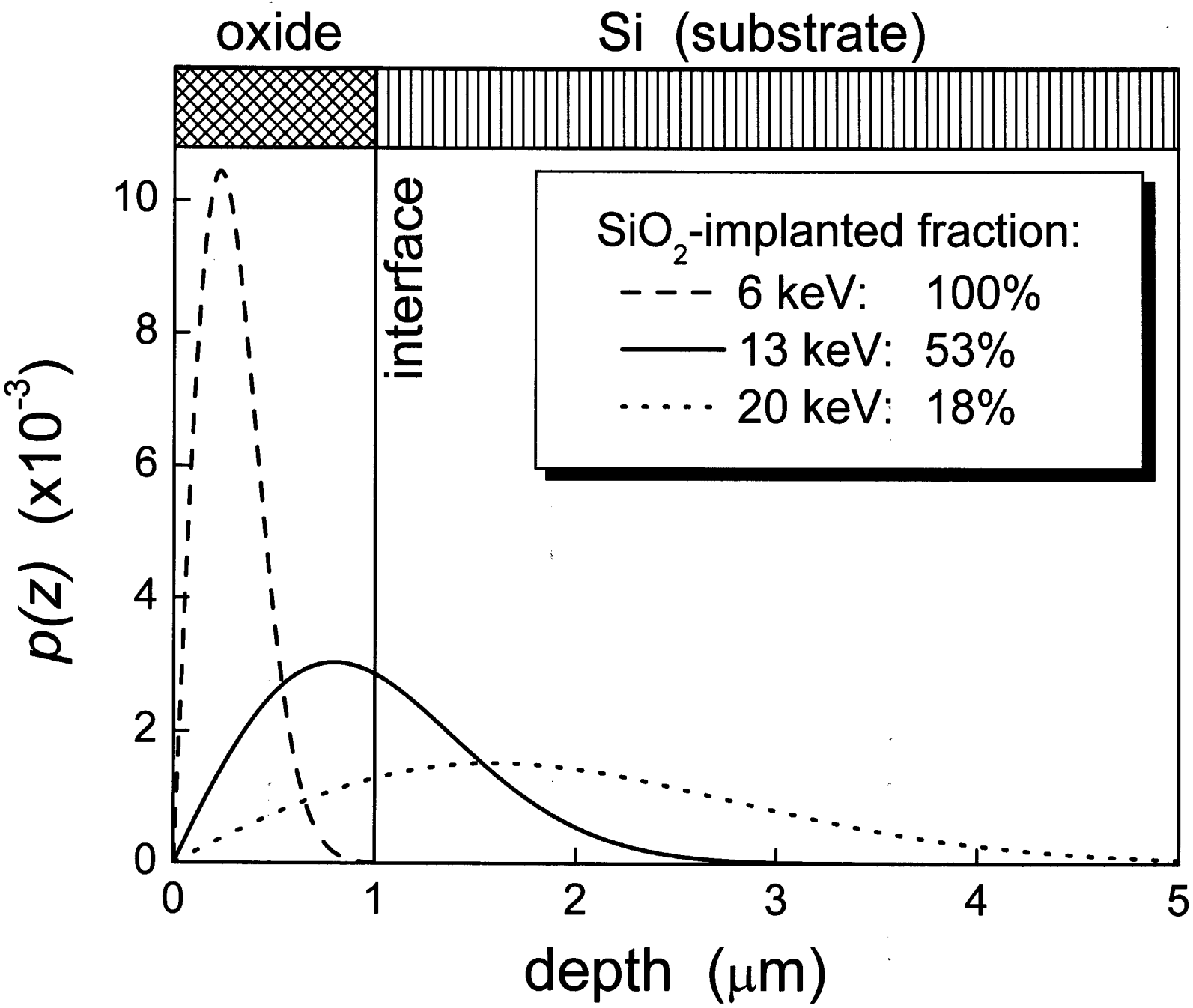

Figure 2 M.P. Petkov *et al.*, *Phys. Rev. B*

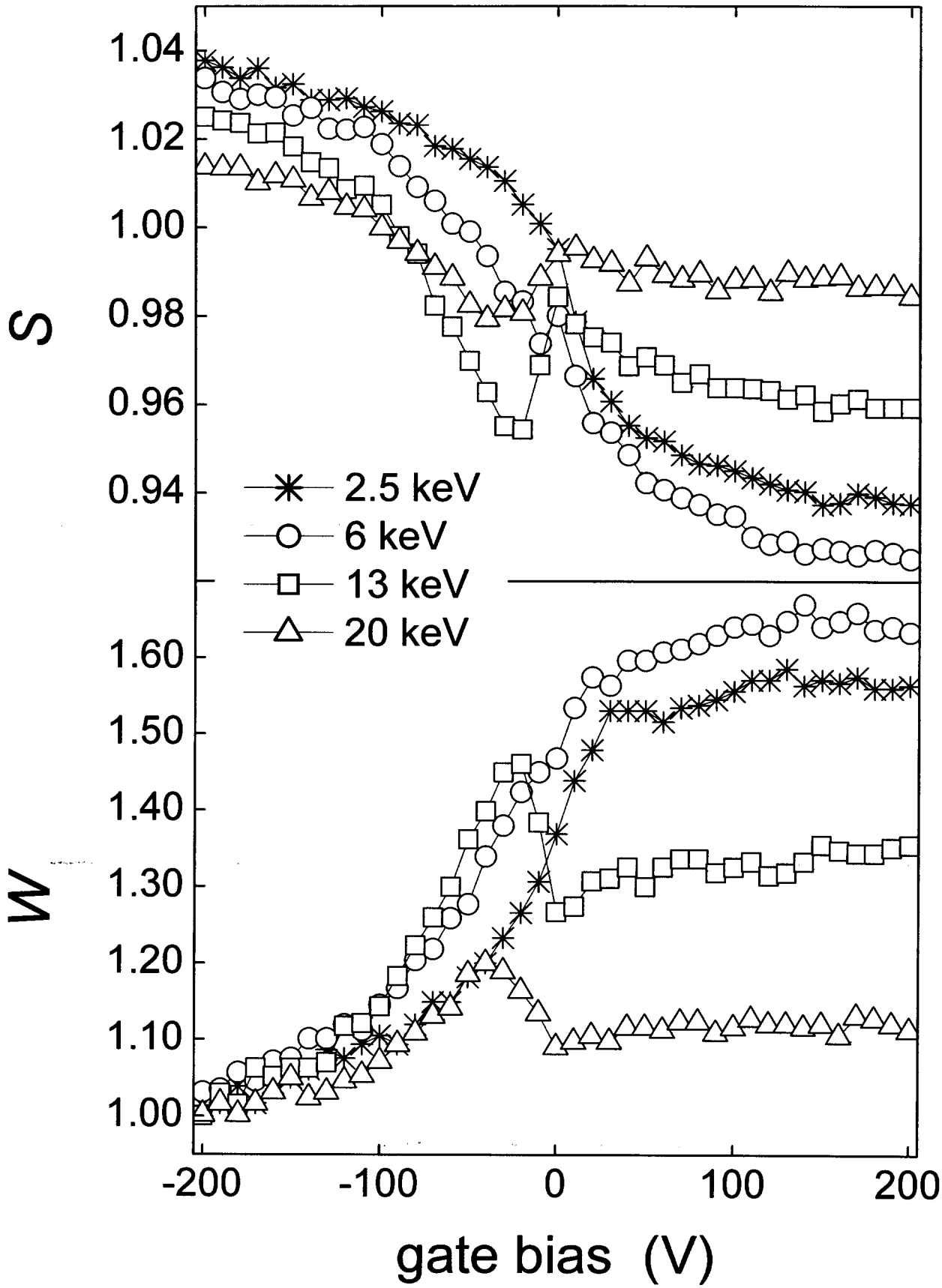

Figure 3 M.P. Petkov *et al.*, *Phys. Rev. B*

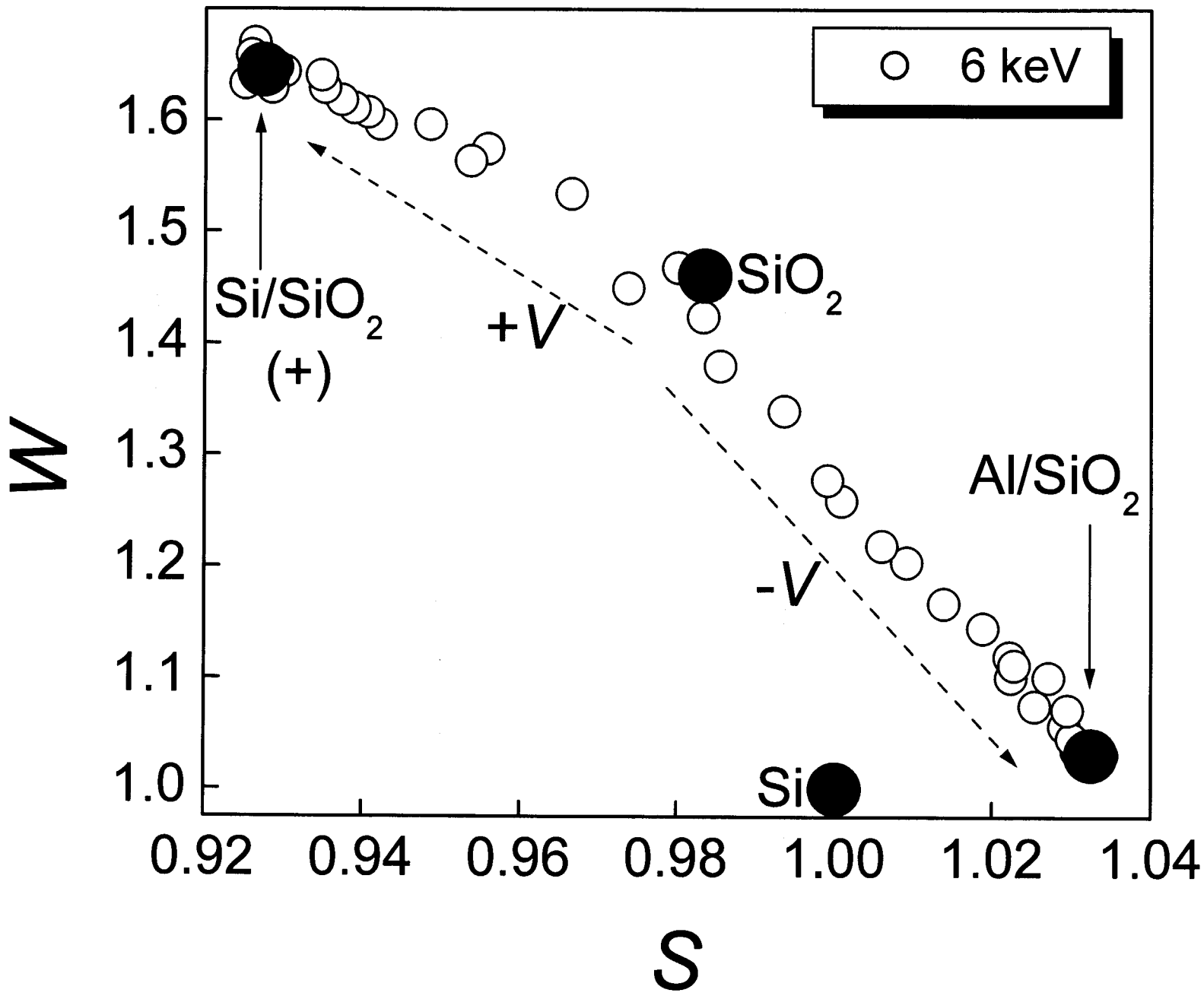

Figure 4 M.P. Petkov *et al.*, *Phys. Rev. B*

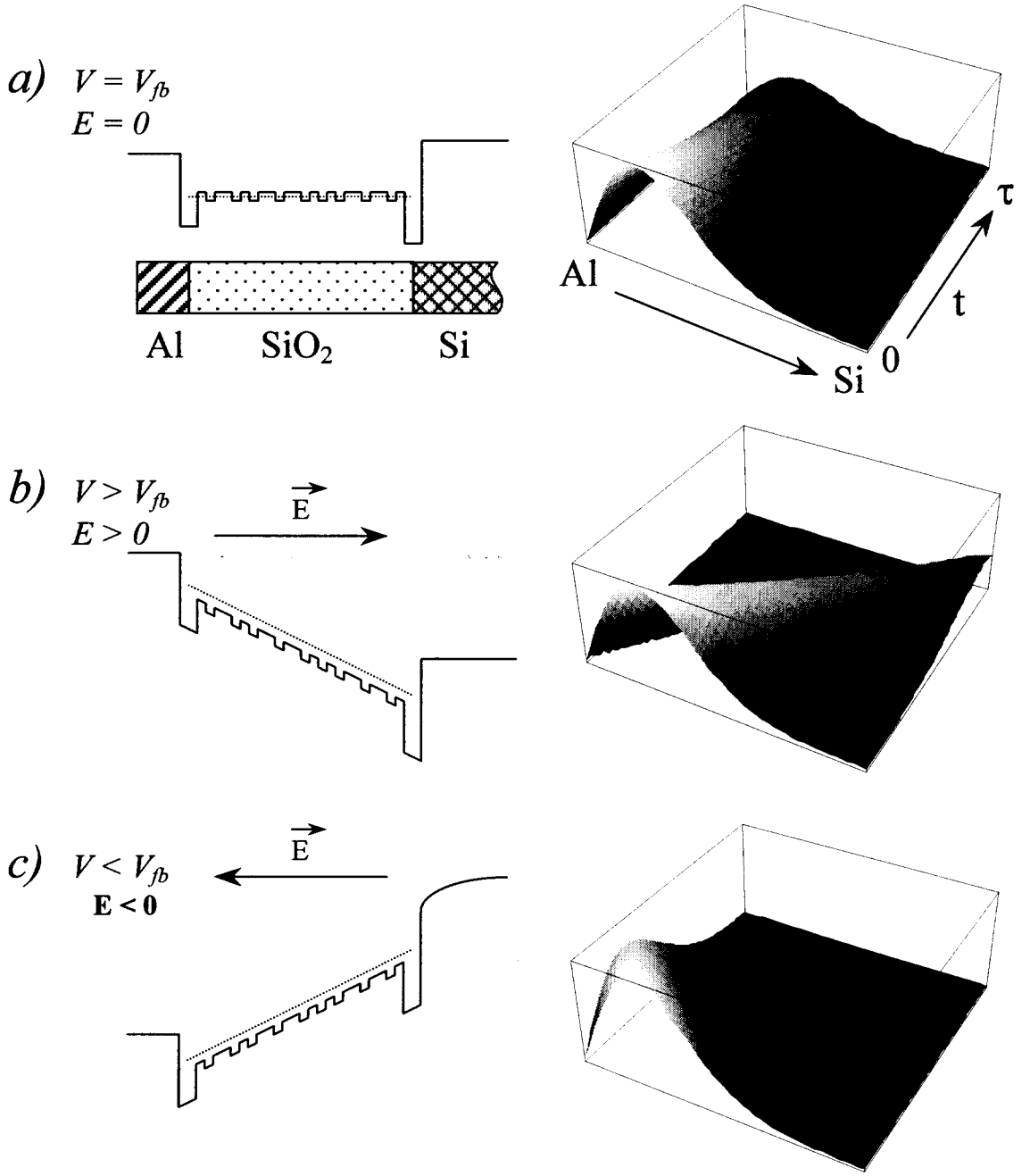

Figure 5 M.P. Petkov *et al.*, *Phys. Rev. B*

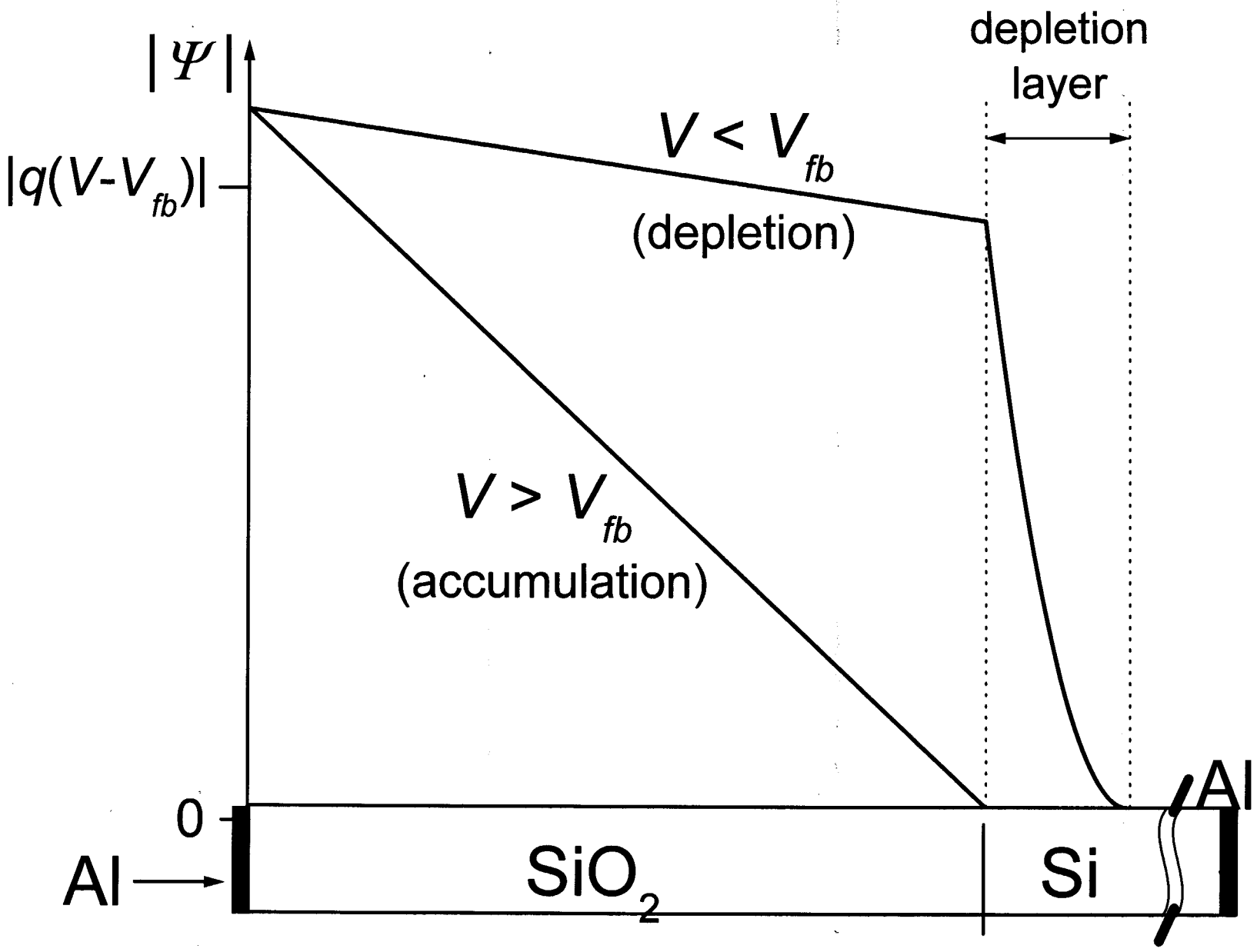

Figure 6 M.P. Petkov *et al.*, *Phys. Rev. B*

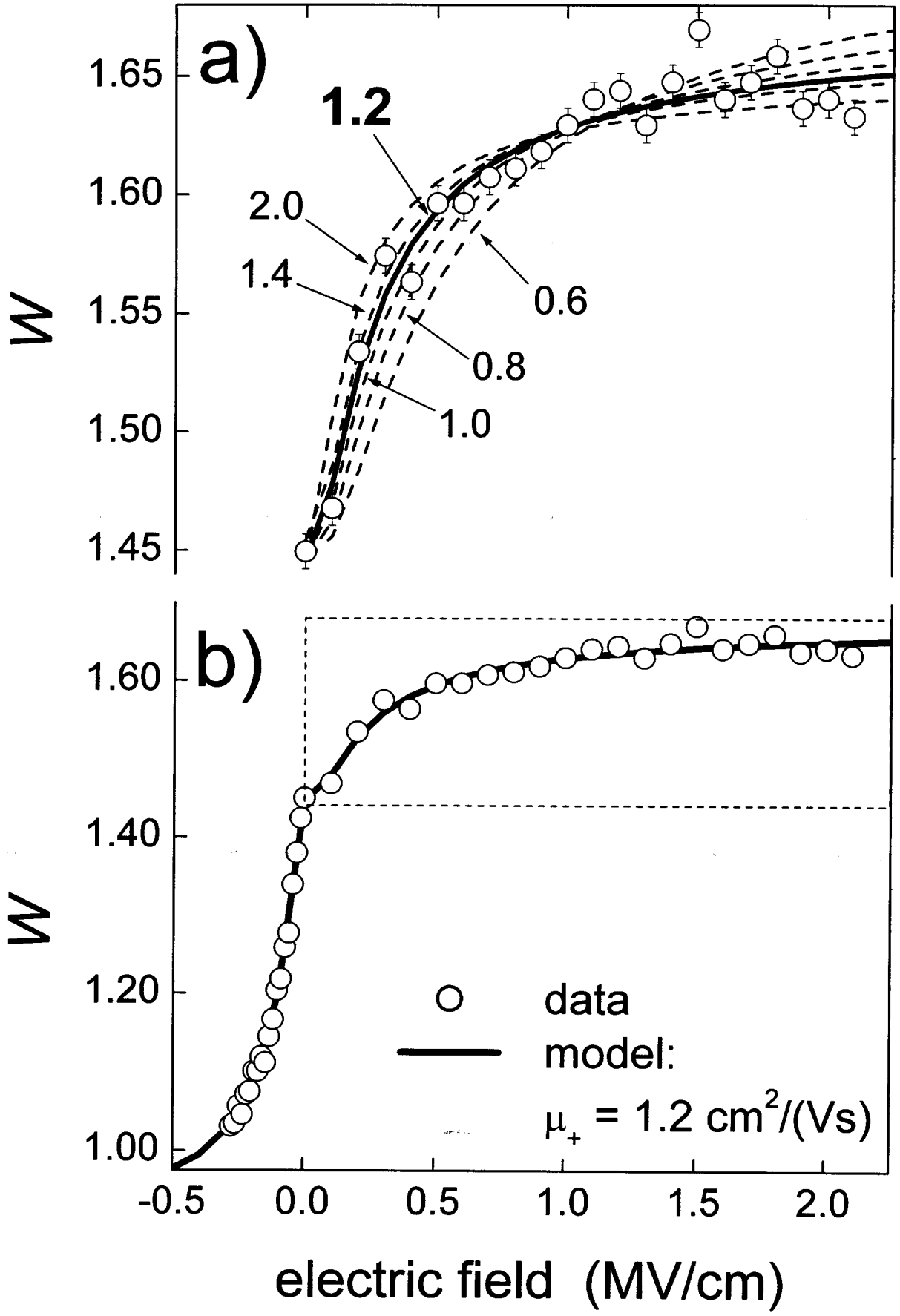

Figure 7 M.P. Petkov *et al.*, *Phys. Rev. B*

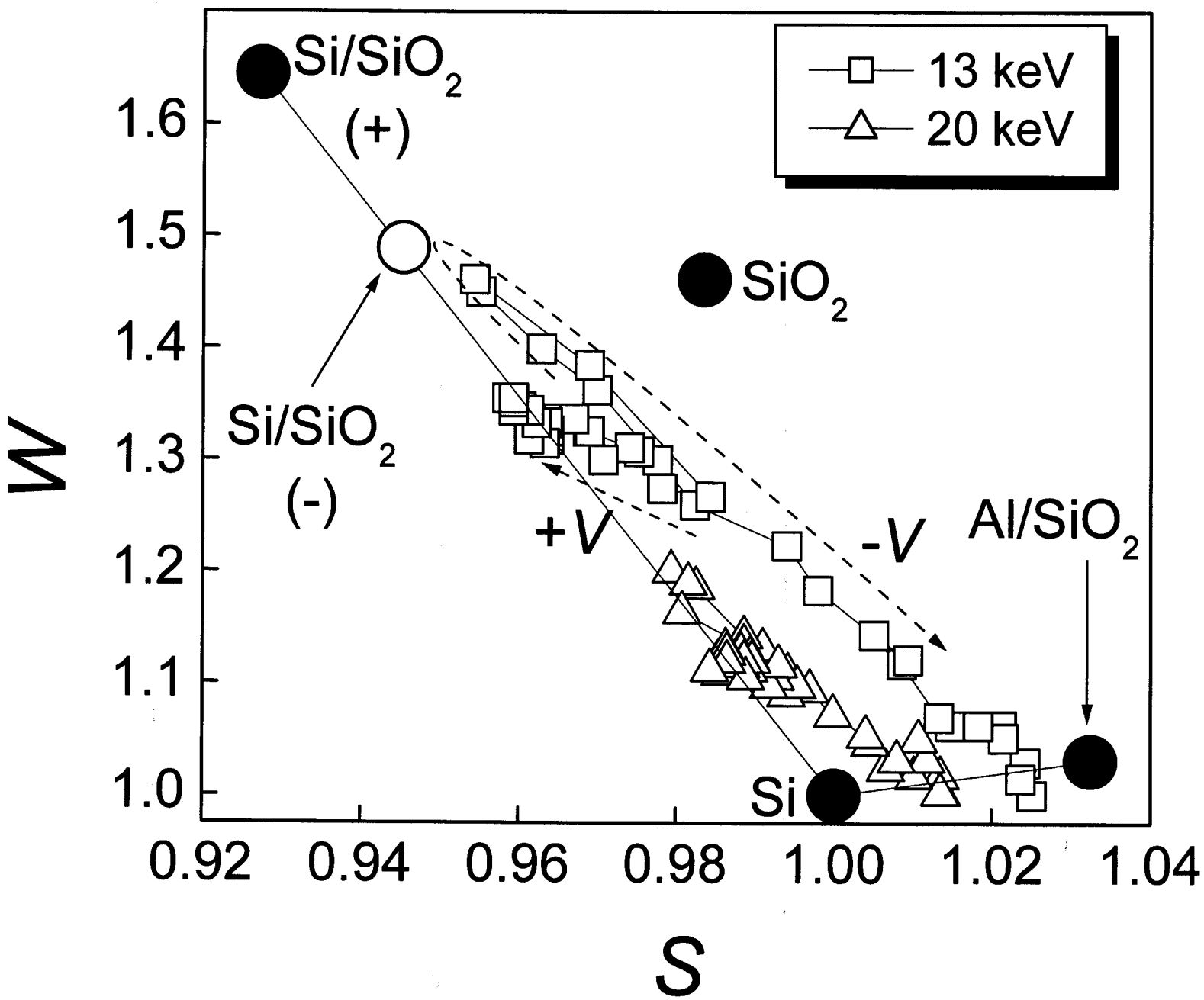

Figure 8 M.P. Petkov *et al.*, *Phys. Rev. B*

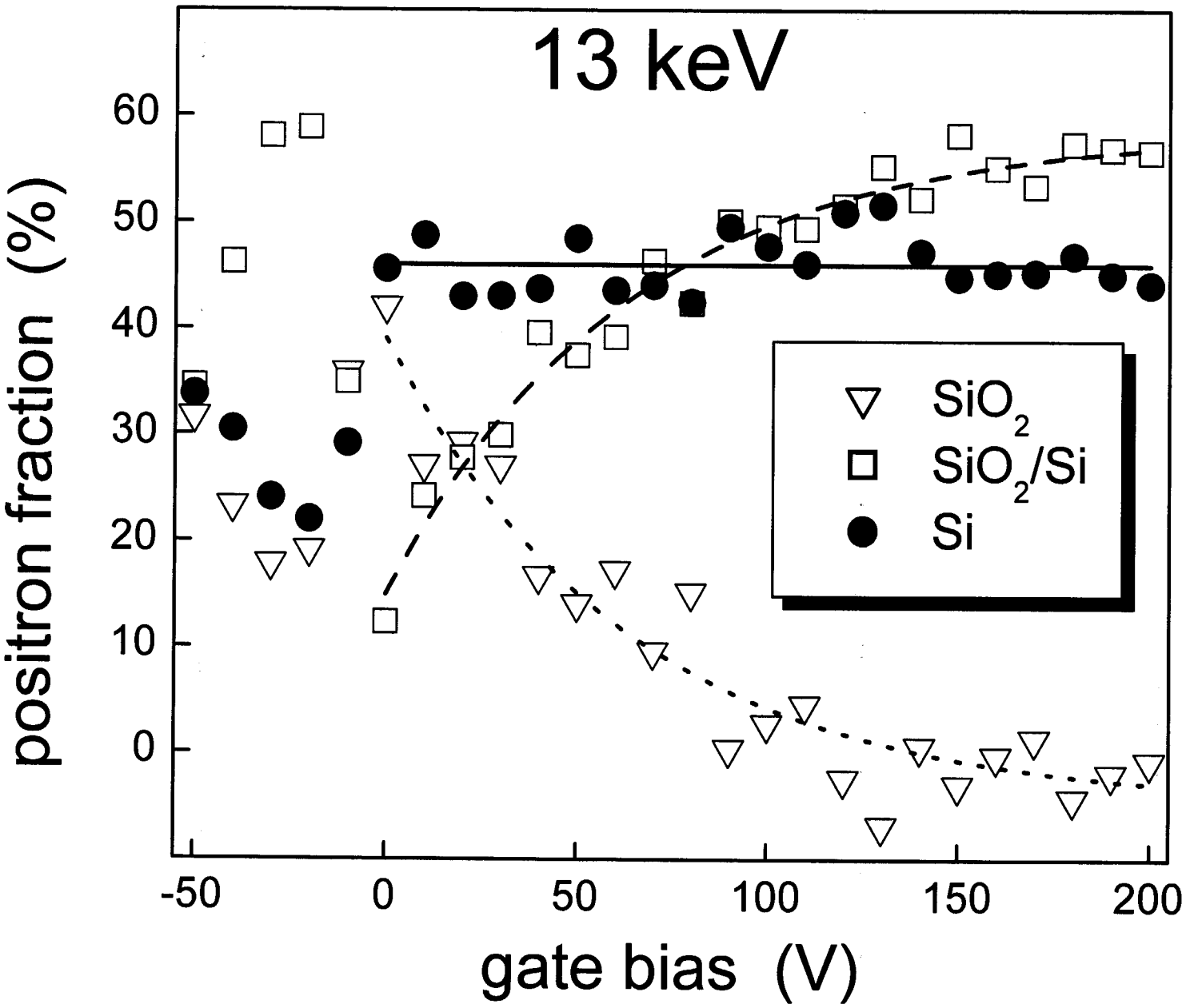

Figure 9 M.P. Petkov *et al.*, *Phys. Rev. B*